JOURNAL OF AIRCRAFT
Vol. 45, No. 3, May–June 2008

Bifurcation Analysis of Aircraft with Structural Nonlinearity and Freeplay Using Numerical Continuation

G. Dimitriadis*
Université de Liège, 4000 Liège, Belgium

DOI: 10.2514/1.28759

In recent years the aeroelastic research community has carried out substantial work on the characterization and prediction of nonlinear aeroelastic phenomena. Of particular interest is the calculation of limit cycle oscillations, which cannot be accomplished using traditional linear methods. In this paper, the prediction of the bifurcation and postbifurcation behavior of nonlinear subsonic aircraft is carried out using numerical continuation. The analysis does not make use of continuation packages such as AUTO or MatCont. Two different continuation techniques are detailed, specifically adapted for realistic aeroelastic models. The approaches are demonstrated on a model of a simple pitch–plunge airfoil with cubic stiffness and an aeroelastic model of a transport aircraft with two different types of nonlinearity in the control surface. It is shown that one of the techniques yields highly accurate predictions for limit cycle oscillation amplitudes and periods while the second method trades off some accuracy for computational efficiency.

I. Introduction

THE prediction of the bifurcation behavior of aircraft is an area of research that is receiving increasing amounts of interest, especially the prediction of bifurcations resulting in limit cycle oscillations (LCO). Bifurcations in aircraft can occur due to a number of nonlinearities that may be present, including structural, aerodynamic, or control nonlinearities. Various methods have been proposed in the past for the prediction of the bifurcation conditions and postbifurcation behavior of nonlinear aircraft, such as the harmonic balance method, normal form [1], center manifold [2], and various types of linearization. Numerical continuation has also been used by some researchers. However, the treatment of numerical continuation by aeroelasticians has always been through software packages such as AUTO [3] and MatCont [4]. Such studies include the piecewise linear work by Roberts et al. [5], the store-induced limit cycle oscillation investigation by Beran et al. [6], the panel flutter work by Gee [7], and other LCO prediction work [8,9]

Although complete packages such as AUTO and MatCont are very comprehensive and can deal with many different types of bifurcation, they were developed for general nonlinear dynamic systems. As such they are not necessarily suitable for very large systems with dozens or even hundreds of states. In this paper numerical continuation is implemented from first principles, without recourse to dedicated packages. It is shown how the method can be applied to aeroelastic models of full aircraft. The method is tailored to be as efficient as possible given the particularities of aeroelastic models. In essence, this paper offers a complete numerical continuation methodology for nonlinear aircraft with linear aerodynamics.

II. Basics of Numerical Continuation

The term numerical continuation is used to denote a class of methods that have been developed over many years, designed to solve nonlinear problems that depend on one or more parameters. The main objective of numerical continuation is the solution of nonlinear algebraic equations of the form

$$\mathbf{f}(\mathbf{x}, \lambda) = \mathbf{0} \tag{1}$$

where $\mathbf{f}$ is a vector containing nonlinear functions, $\mathbf{x}$ is a vector of independent unknowns, and λ is a parameter whose value can vary. Given a known solution $\mathbf{x}_0$ at λ_0, numerical continuation can be used to obtain a new solution $\mathbf{x} + \Delta\mathbf{x}$ at $\lambda_0 + \Delta\lambda$, where $\Delta\lambda$ is a small change in parameter value.

The numerical continuation of nonlinear dynamic systems deals with the solution of the equations of motion of these systems. In this work, it will be assumed that the equations of motion are ordinary differential equations (ODEs) of the form

$$\dot{\mathbf{x}} = \mathbf{f}(\mathbf{x}, \lambda) \tag{2}$$

where $\mathbf{x}(t) = [\,x_1(t) \quad \cdots \quad x_n(t)\,]^T$ is a $n \times 1$ vector of system states and $\mathbf{f} = [\,f_1 \quad \cdots \quad f_n\,]^T$ is a $n \times 1$ vector of functions of $\mathbf{x}$ and the parameter λ. In this context, solving for $\mathbf{f}(\mathbf{x}, \lambda) = \mathbf{0}$ is equivalent to $\dot{\mathbf{x}} = 0$, that is, looking for the system's stationary points or equilibrium points. As the parameter λ is varied it can happen that the behavior of the system changes from decaying toward one or more stationary solutions to admitting periodic solutions, called limit cycle oscillations. This phenomenon is usually called a Hopf bifurcation [10]. In this work, the continuation of such periodic solutions will be mainly considered.

It is assumed that the system of Eq. (2) admits periodic solutions of period T for a range of λ values. The time coordinate can be scaled with respect to the period using

$$\tau = \frac{t}{T} \tag{3}$$

so that Eq. (2) becomes

$$\mathbf{x}' = T\mathbf{f}(\mathbf{x}, \lambda) \tag{4}$$

where the prime denotes differentiation with respect to τ.

The basis of numerical continuation is the reduction of Eq. (4) into a set of nonlinear algebraic equations of the form

$$\mathbf{F}(\mathbf{x}(\tau), \lambda) = \mathbf{0} \tag{5}$$

where $\mathbf{F}$ are nonlinear functions. Then, given an initial guess for $\mathbf{x}(t)$, say $\mathbf{x}_0(t)$, at a particular value of λ, a better value $\mathbf{x}$ can be obtained by solving the Newton system

$$\left.\frac{\partial \mathbf{F}}{\partial \mathbf{x}}\right|_{\mathbf{x}_0(\tau),\lambda} \Delta\mathbf{x}(\tau) = -\mathbf{F}(\mathbf{x}_0(\tau), \lambda) \tag{6}$$

Received 7 November 2006; revision received 21 September 2007; accepted for publication 16 December 2007.

*Assistant Professor, Département d'Aérospatiale et Mécanique, BAT: B52/3, chemin des Chevreuils, 1; gdimitriadis@ulg.ac.be. Member AIAA.

$$\mathbf{x}_1(\tau) = \mathbf{x}_0(\tau) + \Delta\mathbf{x}(\tau) \tag{7}$$

where $\Delta\mathbf{x}$ is an improvement in $\mathbf{x}_0$. The initial guess itself is, in general, the true solution of Eq. (4) at a different value of λ, say λ_0. The Newton system can be reapplied a number of times until $\Delta\mathbf{x}$ converges to a small value.

Several major approaches can be used to transform the differential equation (4) into the algebraic equation (5). The approach used in AUTO consists of guessing the solution of the equations of motion at numerous time instances over one period and defining $\mathbf{F}(\mathbf{x})$ as the difference between these guessed values and the true solution of Eq. (4) [11]. Using this approach the system of Eq. (5) becomes very large; if the solution $\mathbf{x}$ is calculated using a numerical integration method at m time instances the number of unknowns is $n \times m$. Doedel et al. [3] proposed numerous efficient methods for solving the resulting sparse Newton system. Nevertheless, the number of unknowns can quickly become very significant. For example, an aircraft model with 10 structural modes will have 20 structural states and 40 aerodynamic states if unsteady aerodynamics with four lags are used. If 200 time steps are used in one period then the total number of unknowns is 12,000. By default, AUTO 2000 restricts the problem size to 36 states. Therefore, alternative techniques must be sought for aeroelastic problems.

Such an alternative method for the transformation of the differential equations to algebraic equations is the shooting method, which is essentially a boundary value approach. For a solution $\mathbf{x}(\tau)$ to be periodic, the values of the states at the start of the period must be equal to those at the end of the period. Therefore, the numerical continuation scheme becomes a boundary value problem solving

$$\mathbf{x}(0) = \mathbf{x}(1) \tag{8}$$

The first-order system of differential equations becomes a Newton system for

$$\mathbf{F}(\mathbf{x}, T, \lambda) = \mathbf{x}(0) - \mathbf{x}(1) = 0 \tag{9}$$

The function $\mathbf{F}$ is evaluated by choosing an initial condition vector $\mathbf{x}(0)$ and calculating $\mathbf{x}(1)$ using a numerical integration method. Any numerical integration technique, such as Newmark or Runge–Kutta can be used. In essence, the shooting method is a clever application of numerical integration. Starting from a known solution $\mathbf{x}_0(\tau)$ and T_0 at λ_0, the full Newton system at $\lambda = \lambda_0 + \Delta\lambda$ becomes

$$\begin{gathered}\left(\left.\frac{\partial\mathbf{F}}{\partial\mathbf{x}(0)}\right|_{\mathbf{x}_0,T_0,\lambda} \left.\frac{\partial\mathbf{F}}{\partial T}\right|_{\mathbf{x}_0,T_0,\lambda}\right)\begin{pmatrix}\Delta\mathbf{x}\\ \Delta T\end{pmatrix} = -\mathbf{F}(\mathbf{x_0(0)}, T_0, \lambda)\\ \begin{pmatrix}\mathbf{x}_1(0)\\ T_1\end{pmatrix} = \begin{pmatrix}\mathbf{x}_0(0)\\ T_0\end{pmatrix} + \begin{pmatrix}\Delta\mathbf{x}\\ \Delta T\end{pmatrix}\end{gathered} \tag{10}$$

Equations (10) describe n equations with $n + 1$ unknowns. They can be completed using a phase-fixing equation. The simplest and most robust technique is to set one of the elements of $\mathbf{x}(0)$ to be always equal to zero, for example, $x_1(0) = 0$. Evidently, this can be done without loss of generality. Consequently, the number of unknowns reduces to n.

The derivative matrices, $\partial\mathbf{F}/\partial\mathbf{x}(0)$ and $\partial\mathbf{F}/\partial T$, can be calculated analytically if all the nonlinear functions in Eq. (4) are analytic. If this is not the case, two approaches can be followed. The nonanalytic functions can be replaced by analytic approximations, for example, Coulomb friction can be replaced by a hyperbolic tangent function. Specifically for piecewise linear functions, Roberts et al. [5] used the analytic solutions of the linear subsystems to describe the response of the fully nonlinear system.

The other approach is to calculate the derivative matrices numerically. This can be achieved using a simple forward differences scheme. For example, the derivative $\partial\mathbf{F}/\partial\mathbf{x}(0)|_{\mathbf{x}_0,T_0,\lambda}$ can be calculated as

$$\begin{gathered}\frac{1}{\delta x}[\mathbf{F}(\mathbf{x}(0) + \delta\mathbf{x}_1, T_0, \lambda) - \mathbf{F}(\mathbf{x}(0), T_0, \lambda) \quad \cdots\\ \mathbf{F}(\mathbf{x}(0) + \delta\mathbf{x}_n, T_0, \lambda) - \mathbf{F}(\mathbf{x}(0), T_0, \lambda)]\end{gathered} \tag{11}$$

where δx is a small number and $\delta\mathbf{x}_i$ is the ith column of the $n \times n$ matrix $\delta x\mathbf{I}$. Note that, if the first element of $\mathbf{x}(0)$ has been set to zero for phase fixing then the calculation of the Jacobian starts at $i = 2$ and the resulting matrix is of size $n \times (n - 1)$.

The numerical calculation of the derivative matrices can be speeded up by applying a Jacobian updating method [12] such as Broyden's algorithm [13]. Broyden developed a class of "quasi-Newton" methods for the solution of nonlinear algebraic equations that do not require the explicit calculation of the Jacobian at each iteration.

The size of the resulting Newton system is significantly smaller. On the other hand, the Jacobian of Eqs. (10) is not sparse but full; nevertheless, there is no size of aeroelastic model that cannot be treated by the shooting approach.

A. Starting the Continuation Scheme

Nonlinear systems do not always have periodic solutions. Aeroelastic systems, in particular, will generally have decaying responses which bifurcate to limit cycle oscillations at a critical flight condition. At subcritical flight conditions there is no sense in using numerical continuation as described in the previous section. The starting algorithm for the continuation scheme depends on the type of bifurcation that occurs at the critical conditions. The vast majority of studies into nonlinear aeroelastic systems deal with Hopf bifurcations.

The first step is to determine the critical value of the airspeed, or other continuation parameter, at which Hopf bifurcation occurs. It can be shown that, when looking for a Hopf bifurcation, the stability of the full nonlinear system [Eq. (2)] depends on the stability of the linearized system around the equilibrium point, $\mathbf{x}_E$. The equations of motion of this linearized system are given by

$$\dot{\phi} = \left.\frac{\partial\mathbf{f}}{\partial\mathbf{x}}\right|_{\mathbf{x}_E,\lambda}\phi \tag{12}$$

which are first-order, linear, time-invariant ODEs. Therefore, the stability of the nonlinear system can be investigated by calculating the eigenvalues, p, of the matrix $\mathbf{A} = \partial\mathbf{f}/\partial\mathbf{x}|_{\mathbf{x}_E,\lambda}$. If all the eigenvalues have negative real parts then the system is stable and its response amplitude will decay with time. If at least one complex conjugate pair of eigenvalues, p_c, has zero real parts, a Hopf bifurcation has occurred [14]. The parameter value at which this condition is met is the critical parameter value, λ_c. The critical pair of eigenvalues will be of the form $\pm\jmath\omega_c$, where $\jmath = \sqrt{-1}$ and ω_c is the radial frequency of the resulting limit cycle. Therefore, the oscillation period at the Hopf point is $T_c = 2\pi/\omega_c$ [14].

Once the critical value λ_c has been encountered, the LCO continuation scheme can be started. At a condition $\lambda_c + \Delta\lambda$ the solution of the equations of motion are approximated by a sine wave with period ω_c and amplitude parallel to the eigenvectors corresponding to the critical eigenvalue of $\mathbf{A}$ at λ_c, that is,

$$\mathbf{x}(\tau, \lambda_c + \Delta\lambda) = \varepsilon(\mathbf{v}_1 e^{2\pi\jmath\tau} + \mathbf{v}_2 e^{-2\pi\jmath\tau}) \tag{13}$$

where $\mathbf{v}_1$ is the eigenvector of $\mathbf{A}$ corresponding to the $\jmath\omega_c$ eigenvalue, $\mathbf{v}_2$ is the eigenvector corresponding to the $-\jmath\omega_c$ eigenvalue, and ε is a small positive real scalar. Choosing $\varepsilon = \sqrt{\Delta\lambda}$ will, in general, yield an initial guess good enough to allow the Newton system to converge to the true periodic solution at $\lambda_c + \Delta\lambda$.

B. Arclength Continuation

The numerical continuation scheme described in the previous sections is the most basic scheme available. It is usually called "natural parameter continuation" because the continuation parameter is also the system parameter. For nonlinear problems the number of real solutions is not constant. Solution branches can appear,

disappear, or intersect at different values of the natural parameter. Additionally, solution branches may undergo folds, that is, changes of direction in parameter space. Bifurcation and fold points are collectively known as singularities [15]. Natural parameter continuation will fail at singularity points.

A more robust continuation strategy is the so-called arclength continuation. In this case, the chosen continuation parameter is not λ but the distance s, traveled along the branch being followed. The numerical continuation is preformed in small steps of Δs instead of small steps of $\Delta\lambda$.

Around the fold, Δs must be small to continue the solution successfully; but away from the fold, a small value of Δs is not necessary and computationally inefficient. This is usually achieved by means of pseudoarclength continuation [11]. The pseudoarclength is defined in terms of the rate of change of $\mathbf{x}(0)$, T, and λ with s as

$$\left.\frac{\partial \mathbf{x}(0)^T}{\partial s}\right|_{\mathbf{x}_0,T_0,\lambda_0}\Delta\mathbf{x}+\left.\frac{\partial T}{\partial s}\right|_{\mathbf{x}_0,T_0,\lambda_0}\Delta T+\left.\frac{\partial \lambda}{\partial s}\right|_{\mathbf{x}_0,T_0,\lambda_0}\Delta\lambda=\Delta s \quad (14)$$

and $\Delta\lambda$ is now treated as an additional unknown so that the pseudoarclength form of the Newton system becomes

$$\begin{pmatrix} \left.\frac{\partial \mathbf{F}}{\partial \mathbf{x}(0)}\right|_{\mathbf{x}_0,T_0,\lambda_0} & \left.\frac{\partial \mathbf{F}}{\partial T}\right|_{\mathbf{x}_0,T_0,\lambda_0} & \left.\frac{\partial \mathbf{F}}{\partial \lambda}\right|_{\mathbf{x}_0,T_0,\lambda_0} \\ \left.\frac{\partial \mathbf{x}(0)^T}{\partial s}\right|_{\mathbf{x}_0,T_0,\lambda_0} & \left.\frac{\partial T}{\partial s}\right|_{{}_0\mathbf{x}_0,T_0,\lambda_0} & \left.\frac{\partial \lambda}{\partial s}\right|_{{}_0\mathbf{x}_0,T_0,\lambda_0} \end{pmatrix}\begin{pmatrix}\Delta\mathbf{x}\\ \Delta T\\ \Delta\lambda\end{pmatrix} = \begin{pmatrix}-\mathbf{F}(\mathbf{x_0}(\mathbf{0}),T_0,\lambda_0)\\ \Delta s\end{pmatrix} \quad (15)$$

$$\begin{pmatrix}\mathbf{x}_1(0)\\ T_1\\ \lambda_1\end{pmatrix}=\begin{pmatrix}\mathbf{x}_0(0)\\ T_0\\ \lambda_0\end{pmatrix}+\begin{pmatrix}\Delta\mathbf{x}\\ \Delta T\\ \Delta\lambda\end{pmatrix}$$

which is a system of $n+1$ equations with $n+1$ unknowns. The initial direction vectors are assumed to be known. Once the solution $\mathbf{x}$ at conditions T, λ has converged, new direction vectors can be calculated from the following system of equations:

$$\begin{pmatrix} \left.\frac{\partial \mathbf{F}}{\partial \mathbf{x}(0)}\right|_{\mathbf{x},T,\lambda} & \left.\frac{\partial \mathbf{F}}{\partial T}\right|_{\mathbf{x},T,\lambda} & \left.\frac{\partial \mathbf{F}}{\partial \lambda}\right|_{\mathbf{x},T,\lambda} \\ \left.\frac{\partial \mathbf{x}(0)}{\partial s}\right|^T_{\mathbf{x}_0,T_0,\lambda_0} & \left.\frac{\partial T}{\partial s}\right|_{\mathbf{x}_0,T_0,\lambda_0} & \left.\frac{\partial \lambda}{\partial s}\right|_{\mathbf{x}_0,T_0,\lambda_0} \end{pmatrix}\begin{pmatrix} \left.\frac{\partial \mathbf{x}(0)}{\partial s}\right|_{\mathbf{x},T,\lambda}\\ \left.\frac{\partial T}{\partial s}\right|_{\mathbf{x},T,\lambda}\\ \left.\frac{\partial \lambda}{\partial s}\right|_{\mathbf{x},T,\lambda}\end{pmatrix}=\begin{pmatrix}\mathbf{0}\\ 1\end{pmatrix} \quad (16)$$

Notice that the second line of Eq. (16) is an approximation of Eq. (14). As such, the new direction vectors will not have length exactly equal to 1. This can be achieved by rescaling them by a scalar a equal to

$$a=\sqrt{\left.\frac{\partial \mathbf{x}(0)}{\partial s}\right|^T_{\mathbf{x},T,\lambda}\left.\frac{\partial \mathbf{x}(0)}{\partial s}\right|_{\mathbf{x},T,\lambda}+\left.\frac{\partial T}{\partial s}\right|^2_{\mathbf{x},T,\lambda}+\left.\frac{\partial \lambda}{\partial s}\right|^2_{\mathbf{x},T,\lambda}} \quad (17)$$

that is, the length of the approximate total direction vector obtained from Eq. (16).

C. Step Control

The value of the arclength increment, Δs, is a crucial parameter. If it is too high, then the singularity may be missed and continuation may fail. If it is too low, then the continuation scheme becomes unnecessarily slow. In general, as a solution branch is followed, the direction vectors will change length and the solution will advance at a variable rate.

Step control algorithms attempt to normalize the advance rate of the solution so that the arclength increment becomes smaller at areas of high curvature and larger at areas of low curvature. There are several such algorithms but here only the "step length adaptation by asymptotic expansion" [12] method will be considered. The method attempts to fix the rate at which the Newton system converges. Consider the Newton system of Eq. (15) and denote by $\mathbf{u}$ the vector $\mathbf{u}=[\,\Delta\mathbf{x}(0)^T \quad \Delta T^T \quad \Delta\lambda^T\,]^T$. The Newton iterations are stopped when $\sqrt{\mathbf{u}^T\mathbf{u}}<\varepsilon$, where ε is a small positive real number. Denote by $\mathbf{u}_1$ the value of $\mathbf{u}$ at the end of the first iteration and by $\mathbf{u}_2$ its value at the end of the second iteration. A contraction rate can be defined as

$$\kappa=\frac{\sqrt{\mathbf{u}_2^T\mathbf{u}_2}}{\sqrt{\mathbf{u}_1^T\mathbf{u}_1}} \quad (18)$$

so that it represents the speed with which the solution is approached at the first two iterations. It is desired to keep this speed to a constant value $\bar{\kappa}$. Then, once the Newton system has converged and new direction vectors have been calculated, a new arclength increment, $\bar{\Delta}s$ is defined as

$$\bar{\Delta}s=\Delta s\sqrt{\frac{\bar{\kappa}}{\kappa}} \quad (19)$$

In this manner the contraction rate is kept approximately constant as the solution branch is followed.

D. Stability Analysis

Periodic solutions of nonlinear systems can be stable, unstable, or half-stable depending on whether they attract trajectories or not. Formally, for a periodic orbit $\mathbf{x}$ to be stable, the Poincaré stability condition [16] states that

$$\int_0^T \nabla\cdot\mathbf{f}(\mathbf{x})\,\mathrm{d}t<0 \quad (20)$$

where $\nabla\cdot\mathbf{f}$ denotes the divergence such that $\nabla\cdot\mathbf{f}=\partial f_1/\partial x_1+\cdots+\partial f_n/\partial x_n$. Equation (20) can be calculated once a new converged periodic orbit $\mathbf{x}$ with period T at λ has been obtained.

In the case of the shooting method the vector space $\mathbf{f}$ depends only on $\mathbf{x}_0$. Once a converged orbit $\mathbf{x}$ has been obtained, the divergence of $\mathbf{f}$ can be obtained from

$$\nabla\cdot\mathbf{f}(\mathbf{x}_0)=\mathrm{trace}\left(\left.\frac{\partial \mathbf{F}}{\partial \mathbf{x}_0}\right|_{\mathbf{x}_0,T,\lambda}\right) \quad (21)$$

and the Poincaré stability parameter can be estimated from the sum of the elements of $\nabla\cdot\mathbf{f}(\mathbf{x}_0)$.

III. Incremental Numerical Continuation

Incremental numerical continuation (INC) is proposed here as a faster and less memory intensive continuation scheme, designed to avoid the Newton–Raphson iteration at each value of the continuation parameter, at the expense of accuracy. As before, the equations of motion are scaled with respect to the period and it is assumed that they have a known periodic solution, $\mathbf{x}_0(t)$ at λ_0 with a period T_0, such that Eq. (4) becomes

$$\mathbf{x}_0'=T_0\mathbf{f}(\mathbf{x}_0,\lambda_0) \quad (22)$$

It is desired to calculate other solutions $\mathbf{x}$ in the neighborhood of λ_0. The main assumption underlying this calculation is that the derivative of $\mathbf{f}$ with respect to λ is continuous and finite in the neighborhood. Then, if λ_0 is increased by a small amount $\Delta\lambda$, the changes in $\mathbf{x}$ and T are also small, so that

$$\mathbf{x}=\mathbf{x}_0+\Delta\mathbf{x}, \qquad T=T_0+\Delta T \quad (23)$$

Substituting Eqs. (23) into Eq. (4) yields

$$\mathbf{x}_0'+\Delta\mathbf{x}'=(T_0+\Delta T)\mathbf{f}(\mathbf{x}_0+\Delta\mathbf{x},\lambda_0+\Delta\lambda) \quad (24)$$

Expanding the nonlinear function as a first-order Taylor series around λ_0 yields

$$\mathbf{x}_0' + \Delta\mathbf{x}' = (T_0 + \Delta T)\left(\mathbf{f}(\mathbf{x}_0, \lambda_0) + \left.\frac{\partial \mathbf{f}}{\partial \mathbf{x}}\right|_{\mathbf{x}_0,\lambda_0} \Delta\mathbf{x} + \left.\frac{\partial \mathbf{f}}{\partial \lambda}\right|_{\mathbf{x}_0,\lambda_0} \Delta\lambda\right)$$
$$= T_0\mathbf{C} + T_0\mathbf{A}\Delta\mathbf{x} + T_0\mathbf{B}\Delta\lambda + \mathbf{C}\Delta T \tag{25}$$

where the derivatives of $\mathbf{f}$ with respect to $\mathbf{x}$ (Jacobian) and λ are denoted by

$$\mathbf{A}(\tau) = \left.\frac{\partial \mathbf{f}}{\partial \mathbf{x}}\right|_{\mathbf{x}_0,\lambda_0}, \qquad \mathbf{B}(\tau) = \left.\frac{\partial \mathbf{f}}{\partial \lambda}\right|_{\mathbf{x}_0,\lambda_0}, \qquad \mathbf{C}(\tau) = \mathbf{f}(\mathbf{x}_0, \lambda_0) \tag{26}$$

and terms in $\Delta T\Delta\mathbf{x}$ and $\Delta T\Delta\lambda$ are assumed to be negligible. Noting from Eq. (24) that $\mathbf{x}_0' = T_0\mathbf{C}$ yields

$$\Delta\mathbf{x}' = T_0\mathbf{A}\Delta\mathbf{x} + T_0\mathbf{B}\Delta\lambda + \mathbf{C}\Delta T \tag{27}$$

Equation (27) is a set of n first-order linear differential equations with time-dependent coefficients, to be solved for the unknown changes $\Delta\mathbf{x}$ and ΔT in the periodic solution of Eq. (2) caused by a small change in parameter value $\Delta\lambda$. Notice that, as in the case of the shooting method, the solution $\Delta\mathbf{x}(t)$ depends uniquely on the value of the initial conditions, $\Delta\mathbf{x}(0)$. Therefore, there are n unknown initial conditions and one unknown period perturbation, ΔT, for a total of $n + 1$ unknowns, whereas there are only n equations.

The INC method is based on the discretization of the periodic solution at m discrete points over an entire period. Therefore, $\mathbf{x}_0(\tau)$ is available at m time instances and $\Delta\mathbf{x}$ is to be calculated these same time instances. As the response at $\lambda_0 + \Delta\lambda$ is also assumed to be periodic, it is required that

$$\Delta\mathbf{x}(0) = \Delta\mathbf{x}(1) \tag{28}$$

This condition is the governing equation for the calculation of $\Delta\mathbf{x}$ and ΔT. There are many ways to complete this calculation; here a first-order finite difference scheme is chosen. The derivative of $\Delta\mathbf{x}$ with respect to τ can be expressed as

$$\Delta\mathbf{x}_j' = \frac{\Delta\mathbf{x}_{j+1} - \Delta\mathbf{x}_j}{\tau_{j+1} - \tau_j} = \frac{\Delta\mathbf{x}_{j+1} - \Delta\mathbf{x}_j}{\delta\tau} \tag{29}$$

where the subscript j denotes values at the jth time instance. Substituting into Eq. (27) yields

$$\Delta\mathbf{x}_{j+1} = (\mathbf{I} + \delta\tau T_0\mathbf{A}_j)\Delta\mathbf{x}_j + \delta\tau(T_0\mathbf{B}_j\Delta\lambda + \mathbf{C}_j\Delta T) \tag{30}$$

This is a regression equation that gives the value of $\Delta\mathbf{x}$ at τ_{j+1} in terms of its value at τ_j. For $j = 0$:

$$\Delta\mathbf{x}_1 = (\mathbf{I} + \delta\tau T_0\mathbf{A}_0)\Delta\mathbf{x}_0 + \delta\tau(T_0\mathbf{B}_0\Delta\lambda + \mathbf{C}_0\Delta T)$$

For $j = 1$:

$$\Delta\mathbf{x}_2 = (\mathbf{I} + \delta\tau T_0\mathbf{A}_1)\Delta\mathbf{x}_1 + \delta\tau(T_0\mathbf{B}_1\Delta\lambda + \mathbf{C}_1\Delta T)$$
$$= (\mathbf{I} + \delta\tau T_0\mathbf{A}_1)(\mathbf{I} + \delta\tau T_0\mathbf{A}_0)\Delta\mathbf{x}_0$$
$$+ (\mathbf{I} + \delta\tau T_1\mathbf{A}_1)\delta\tau(T_0\mathbf{B}_0\Delta\lambda + \mathbf{C}_0\Delta T) + \delta\tau(T_0\mathbf{B}_1\Delta\lambda + \mathbf{C}_1\Delta T)$$

For $j = 2$:

$$\Delta\mathbf{x}_3 = (\mathbf{I} + \delta\tau T_0\mathbf{A}_2)\Delta\mathbf{x}_2 + \delta\tau(T_0\mathbf{B}_2\Delta\lambda + \mathbf{C}_2\Delta T)$$
$$= (\mathbf{I} + \delta\tau T_0\mathbf{A}_2)(\mathbf{I} + \delta\tau T_0\mathbf{A}_1)(\mathbf{I} + \delta\tau T_0\mathbf{A}_0)\Delta\mathbf{x}_0$$
$$+ (\mathbf{I} + \delta\tau T_0\mathbf{A}_2)(\mathbf{I} + \delta\tau T_1\mathbf{A}_1)\delta\tau(T_0\mathbf{B}_0\Delta\lambda + \mathbf{C}_0\Delta T)$$
$$+ (\mathbf{I} + \delta\tau T_0\mathbf{A}_2)\delta\tau(T_0\mathbf{B}_1\Delta\lambda + \mathbf{C}_1\Delta T) + \delta\tau(T_0\mathbf{B}_2\Delta\lambda + \mathbf{C}_2\Delta T)$$

By extension it can be seen that

$$\Delta\mathbf{x}_{j+1} = \prod_{i=0}^{j}(\mathbf{I} + \delta\tau T_0\mathbf{A}_{j-i})\Delta\mathbf{x}_0$$
$$+ \sum_{i=0}^{j-1}\prod_{k=0}^{j-i-1}(\mathbf{I} + \delta\tau T_0\mathbf{A}_{j-k})\delta\tau(T_0\mathbf{B}_i\Delta\lambda + \mathbf{C}_i\Delta T)$$
$$+ \delta\tau(T_0\mathbf{B}_j\Delta\lambda + \mathbf{C}_j\Delta T) \tag{31}$$

Equation (31) can be simplified by denoting

$$\mathbf{P}_j = \prod_{i=0}^{j}(\mathbf{I} + \delta\tau T_0\mathbf{A}_{j-i})$$
$$\mathbf{Q}_j = \sum_{i=0}^{j-1}\prod_{k=0}^{j-i-1}(\mathbf{I} + \delta\tau T_0\mathbf{A}_{j-k})\delta\tau\mathbf{C}_i + \delta\tau\mathbf{C}_j \tag{32}$$
$$\mathbf{R}_j = \sum_{i=0}^{j-1}\prod_{k=0}^{j-i-1}(\mathbf{I} + \delta\tau T_0\mathbf{A}_{j-k})\delta\tau T_0\mathbf{B}_i + \delta\tau T_0\mathbf{B}_j$$

yielding

$$\Delta\mathbf{x}_{j+1} = \mathbf{P}_j\Delta\mathbf{x}_0 + \mathbf{Q}_j\Delta T + \mathbf{R}_j\Delta\lambda \tag{33}$$

For $j = m - 1$ this equation becomes

$$\Delta\mathbf{x}_m = \mathbf{P}_{m-1}\Delta\mathbf{x}_0 + \mathbf{Q}_{m-1}\Delta T + \mathbf{R}_{m-1}\Delta\lambda \tag{34}$$

Substituting Eq. (34) into Eq. (28) yields

$$(\mathbf{I} - \mathbf{P}_{m-1})\Delta\mathbf{x}_0 - \mathbf{Q}_{m-1}\Delta T = \mathbf{R}_{m-1}\Delta\lambda \tag{35}$$

which is a linear system of n algebraic equations for the $n + 1$ unknowns $\Delta\mathbf{x}_0$ and ΔT. To complete the system of equations a phase-fixing condition must be introduced. One such condition is the Poincaré phase condition, given by

$$(\mathbf{x}(0) - \mathbf{x}_0(0))^T\mathbf{x}_0'(0) = 0 \tag{36}$$

which can be easily transformed to

$$\mathbf{C}_0^T\Delta\mathbf{x}_0 = 0 \tag{37}$$

Thus, the final system of equations becomes

$$\begin{pmatrix} (\mathbf{I} - \mathbf{P}_{m-1}) & -\mathbf{Q}_{m-1} \\ \mathbf{C}_0^T & 0 \end{pmatrix}\begin{Bmatrix} \Delta\mathbf{x}_0 \\ \Delta T \end{Bmatrix} = \begin{Bmatrix} \mathbf{R}_{m-1}\Delta\lambda \\ 0 \end{Bmatrix} \tag{38}$$

Phase fixing can also be performed using a predictor–corrector approach [17] but this is a slower process and is not considered in this work.

Equation (38) is the basis of the INC scheme. Once an accurate periodic solution has been calculated, Eq. (38) can be used to continue this solution for different values of the controlling parameter, λ. The algorithm can be written as follows:

1) Obtain a periodic solution of the system under investigation.

2) Extract one full period's worth of data, $\mathbf{x}_0$, and calculate the period, T_0.

3) While $\lambda < \lambda_{\max}$

Calculate the matrices $\mathbf{A}$, $\mathbf{B}$, and $\mathbf{C}$.

Solve Eq. (38) for the initial conditions $\Delta\mathbf{x}_0$ and period increment ΔT.

Calculate $\Delta\mathbf{x}$ from Eq. (30).

Set $\lambda_0 = \lambda_0 + \Delta\lambda$.

Set $\mathbf{x}_0 = \mathbf{x}_0 + \Delta\mathbf{x}$.

Set $T_0 = T_0 + \Delta T$.

4) End.

$\lambda_{\max}$ is the maximum value of λ for which the solution is to be continued. It can be seen that the method does not attempt to ensure that $\mathbf{x}_0 + \Delta\mathbf{x}$ is an exact solution of the equations of motion; each

continuation step approximates the exact solution and the accuracy of this approximation increases with decreasing $\Delta\lambda$. As there are no Newton–Raphson iterations the method is very fast but requires more continuation steps because $\Delta\lambda$ must be significantly smaller than in the case of the shooting method.

A. Pseudoarclength Continuation

The incremental numerical continuation scheme can be used in conjunction with a pseudoarclength parameter in a manner very similar to that demonstrated in Sec. III.B. In the case of the INC method the unknowns are the increments in the values of $\mathbf{x}(0)$ and the increment in the period. The increments $\Delta\mathbf{x}_0$ cannot be used directly to define an arclength, only a change in arclength. Therefore, the initial values $\mathbf{x}_0$ are used to define the pseudoarclength, as was done for the shooting method.

The pseudoarclength form of the INC equations becomes

$$\begin{pmatrix} (\mathbf{I}-\mathbf{P}_{m-1}) & -\mathbf{Q}_{m-1} & -\mathbf{R}_{m-1} \\ \mathbf{C}_0^T & 0 & 0 \\ \left.\frac{\partial \mathbf{x}(0)^T}{\partial s}\right|_{\mathbf{x}_0,T_0,\lambda_0} & \left.\frac{\partial T}{\partial s}\right|_{\mathbf{x}_0,T_0,\lambda_0} & \left.\frac{\partial \lambda}{\partial s}\right|_{\mathbf{x}_0,T_0,\lambda_0} \end{pmatrix} \begin{Bmatrix} \Delta\mathbf{x}_0 \\ \Delta T \\ \Delta\lambda \end{Bmatrix} = \begin{Bmatrix} \mathbf{0} \\ 0 \\ \Delta s \end{Bmatrix} \tag{39}$$

The new direction vectors can be calculated from the increments $\Delta\mathbf{x}_0$, ΔT, $\Delta\lambda$, and Δs as

$$\left.\frac{\partial \mathbf{x}(0)}{\partial s}\right|_{\mathbf{x},T,\lambda} = \frac{\Delta\mathbf{x}_0}{\Delta s} \qquad \left.\frac{\partial T}{\partial s}\right|_{\mathbf{x},T,\lambda} = \frac{\Delta T}{\Delta s} \qquad \left.\frac{\partial \lambda}{\partial s}\right|_{\mathbf{x},T,\lambda} = \frac{\Delta\lambda}{\Delta s} \tag{40}$$

and then scaled by parameter a in Eq. (17) to ensure that the length of the total direction vector is 1.

B. Stability Analysis

The Poincaré stability condition of Eq. (20) can be readily evaluated from INC calculations. The Jacobian, $\mathbf{A}(\tau)$, of function $\mathbf{f}(\mathbf{x}_0)$ is obtained from Eq. (26) as part of these calculations. The divergence of $\mathbf{f}(\mathbf{x}_0)$ can be easily evaluated from $\nabla\cdot\mathbf{f}(\mathbf{x}_{0_j}) = \text{trace}(\mathbf{A}_j)$ where trace denotes the sum of the diagonal elements of a square matrix. The Poincaré condition approximately becomes

$$\sum_{j=1}^{m} \text{trace}(\mathbf{A}_j) < 0 \tag{41}$$

Notice that in previous calculations $\mathbf{A}_j$ is only available for the starting orbit $\mathbf{x}_0$. Therefore, $\mathbf{A}_j$ must be recalculated for the current orbit $\mathbf{x}_0 + \Delta\mathbf{x}$.

A much faster approximate estimation of the stability of a periodic orbit can be obtained by considering a small disturbance. For a periodic orbit to be stable, trajectories starting from initial conditions close to the orbit should always end up on the orbit itself as time tends to infinity. Define a set of initial conditions $\Delta\bar{\mathbf{x}}(0)$ such that

$$\Delta\bar{\mathbf{x}}(0) = \Delta\mathbf{x}(0) + \boldsymbol{\varepsilon} \tag{42}$$

where $\boldsymbol{\varepsilon}$ is a $n\times 1$ vector of magnitude much smaller than $\Delta\mathbf{x}(0)$. The initial conditions $\Delta\bar{\mathbf{x}}(0)$ will cause the system to follow a trajectory $\Delta\bar{\mathbf{x}}(t)$. If the periodic orbit $\Delta\mathbf{x}(t)$ is stable then

$$\lim_{t\to\infty} \Delta\bar{\mathbf{x}}(t) - \Delta\mathbf{x}(t) = 0$$

An equivalent condition can be used to speed up calculations, looking at the behavior of the trajectory $\Delta\bar{\mathbf{x}}(t)$ over a single period. For stability, $\Delta\bar{\mathbf{x}}(T)$ must be closer to $\Delta\mathbf{x}(T)$ than $\Delta\bar{\mathbf{x}}(0)$ is to $\Delta\mathbf{x}(0)$. This can be written as

$$\begin{aligned}&(\Delta\bar{\mathbf{x}}(T) - \Delta\mathbf{x}(T))^T(\Delta\bar{\mathbf{x}}(T) - \Delta\mathbf{x}(T)) \\ &\quad < (\Delta\bar{\mathbf{x}}(0) - \Delta\mathbf{x}(0))^T(\Delta\bar{\mathbf{x}}(0) - \Delta\mathbf{x}(0))\end{aligned} \tag{43}$$

From Eq. (34), $\Delta\bar{\mathbf{x}}(T)$ is estimated by $\Delta\bar{\mathbf{x}}_m$, which can be obtained as

$$\Delta\bar{\mathbf{x}}_m = \mathbf{P}_{m-1}\bar{\Delta}\mathbf{x}_0 + \mathbf{Q}_{m-1}\Delta T + \mathbf{R}_{m-1} \tag{44}$$

so that Eq. (43) can be rewritten as

$$\boldsymbol{\varepsilon}^T\mathbf{P}_{m-1}^T\mathbf{P}_{m-1}\boldsymbol{\varepsilon} < \boldsymbol{\varepsilon}^T\boldsymbol{\varepsilon} \tag{45}$$

This calculation can be performed numerically, for example, by setting $\boldsymbol{\varepsilon} = 0.1\Delta\mathbf{x}(0)$ and checking whether Eq. (45) is true.

A more thorough but computationally expensive way of assessing the stability of the trajectory is to use the Floquet theory. According to this theory the trajectory is stable if the eigenvalues of the monodromy matrix, $\mathbf{M}$, all lie inside the unit circle, that is, their magnitudes are less than 1. For the discrete representation considered here the monodromy matrix is given by

$$\mathbf{M} = \exp\left(\delta\tau\sum_{i=1}^{m}\mathbf{A}_i\right) \tag{46}$$

where exp denotes the matrix exponential. The advantage of using the monodromy matrix as a stability criterion is that, by examining the behavior of its eigenvalues, the changes in stability can be explained.

IV. Implementation

All the algorithms described previously were implemented using a combination of Matlab and Matlab-compatible C code (mex files). The Matlab interface was used to define the system and to set the continuation and simulation parameters. The numerical integrations were carried out using the mex file by means of a fifth-order Runge–Kutta scheme [18]. The continuation results were produced effectively and efficiently even for a realistic aeroelastic system with 42 states. The codes developed were run on a 1.25-GHz G4 Powerbook with 1.25 MB of RAM; in other words, the computational requirements are very light, even for the largest aeroelastic model treated later in this paper.

V. Pitch–Plunge Airfoil Model

In this section, the two continuation methods outlined previously are applied to the pitch–plunge airfoil aeroelastic model. This model has been used for aeroelastic research since the Theodorsen era and has found applications in the investigation of nonlinear aeroelasticity over the last two decades. Lee et al. [19,20] used the pitch–plunge airfoil with cubic and other nonlinear stiffnesses to demonstrate some basic nonlinear aeroelastic phenomena. Tang et al. [21] and Liu and Dowell [22] used a version of the same airfoil with a control surface to demonstrate secondary bifurcations and to apply a higher order harmonic balance method, respectively. More recently, Millman et al. [23] used the pitch–plunge airfoil to analyze chaotic bifurcations and Baldelli et al. [24] demonstrated a robust solution method for aeroelastic systems containing uncertainties. Marsden and Price [25] built a wind-tunnel model of the nonlinear airfoil and compared the responses to simulation results. Lee et al. [26] returned to the simulated model with cubic stiffness to investigate the effectiveness of higher order harmonic balance methods and to investigate bifurcations in the presence of two cubic springs [27].

The pitch–plunge airfoil without control surface, as investigated by Lee et al. [26,27], will be the subject of the application of continuation methods in this paper. It consists of a two-dimensional airfoil with pitch and plunge degrees of freedom, restrained by torsion and extension springs, respectively; both of these springs can be nonlinear. The aerodynamic forces are calculated using incompressible, inviscid, thin airfoil, unsteady assumptions. The equations of motion for the system are

$$\begin{pmatrix} c_0 & c_1 \\ d_0 & d_2 \end{pmatrix}\begin{pmatrix} \xi'' \\ \alpha'' \end{pmatrix} + \begin{pmatrix} c_2 & c_3 \\ d_2 & d_3 \end{pmatrix}\begin{pmatrix} \xi' \\ \alpha' \end{pmatrix} + \begin{pmatrix} c_4 + c_{10} & c_5 \\ d_4 & d_5 + d_{10} \end{pmatrix}\begin{pmatrix} \xi \\ \alpha \end{pmatrix} + \begin{pmatrix} c_6 & c_7 & c_8 & c_9 \\ d_6 & d_7 & d_8 & d_9 \end{pmatrix}\begin{pmatrix} w_1 \\ w_2 \\ w_3 \\ w_4 \end{pmatrix} + \begin{pmatrix} c_{10}\gamma\xi^3 \\ d_{10}\beta\alpha^3 \end{pmatrix} = \mathbf{0} \tag{47}$$

where ξ is the nondimensional plunge displacement, α is the pitch angle in rad, the (prime) denotes differentiation with respect to nondimensional time, and γ and β are cubic stiffness coefficients. The coefficients c_i, d_i are given in several (if not all) of the publications mentioned previously but are included as an Appendix to this paper for completeness.

In Lee et al. [26], results from this model are presented for the case where $\mu = 100$, $r_\alpha = 0.5$, $a_h = -0.5$, $\zeta_\xi = \zeta_\alpha = 0$, $x_\alpha = 0.25$, $\bar{\omega} = 0.2$, $\beta = 80$, and $\gamma = 0$. Lee et al. used numerical integration to solve Eq. (47); they observed an initial Hopf bifurcation leading to limit cycle oscillations at the linear flutter speed U_L^*, followed by a jump in LCO amplitude and frequency at around $U^*/U_L^* = 2$. This jump occurred at slightly different airspeeds, depending on the initial conditions used for the numerical integration [26,27]. Numerical integration did not reveal the cause of this jump and neither did the harmonic balance analysis they performed. The numerical integration results, recalculated by this author, are shown in Fig. 1. The maximum plunge amplitude, pitch amplitude, and LCO frequency are plotted at several postcritical airspeeds. The jump at around $U^*/U_L^* = 2$ is clearly visible.

The power of numerical continuation lies not only in quickly estimating LCO amplitude and frequency for many parameter values but also in fully characterizing all the bifurcation phenomena occurring in the parameter space of interest. Here, the shooting method was applied to Eq. (47). The results from this application are plotted in Fig. 2, along with the numerical integration results of Fig. 1. The method detected a supercritical Hopf bifurcation at $U_L^* = 6.29$, followed by a fold bifurcation, which causes the jump effect observed by Lee et al. The LCO branch reaches a maximum airspeed ratio of 2.35, at which point it becomes unstable and folds over toward decreasing airspeed values. The branch becomes stable again and folds toward positive airspeed values at $U^*/U_L^* = 1.85$. This means that between airspeed ratios of 1.85 and 2.35 the system can undergo two possible stable limit cycles. Which one it will eventually follow depends on initial conditions. Numerical continuation has provided a complete explanation of the jump phenomenon observed by Liu et al. and left unexplained by numerical integration and harmonic balance analysis. It should be noted, however, that a higher order harmonic balance method could have yielded results similar to those presented in Fig. 2 but only if it was implemented within a continuation framework [28].

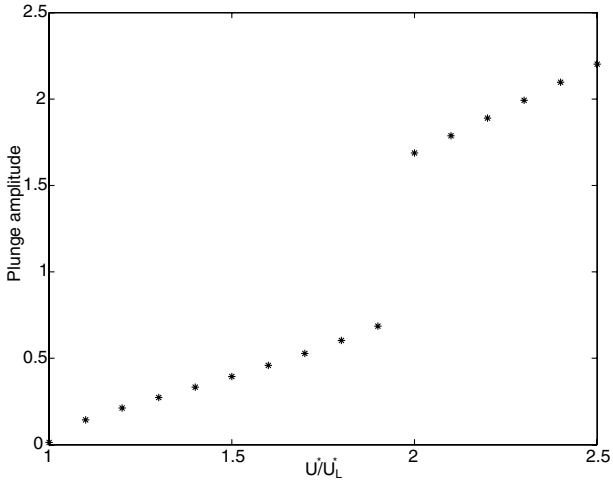

a) Maximum plunge amplitude

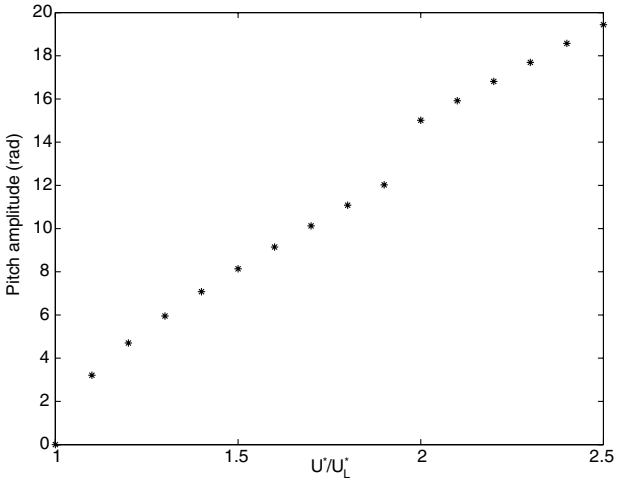

b) Maximum pitch amplitude

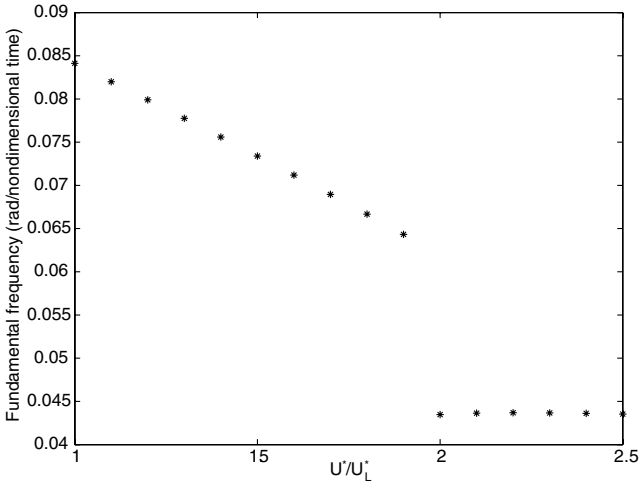

c) LCO frequency

Fig. 1 Numerical integration results for pitch–plunge airfoil with $\beta = 80$, $\gamma = 0$ [26].

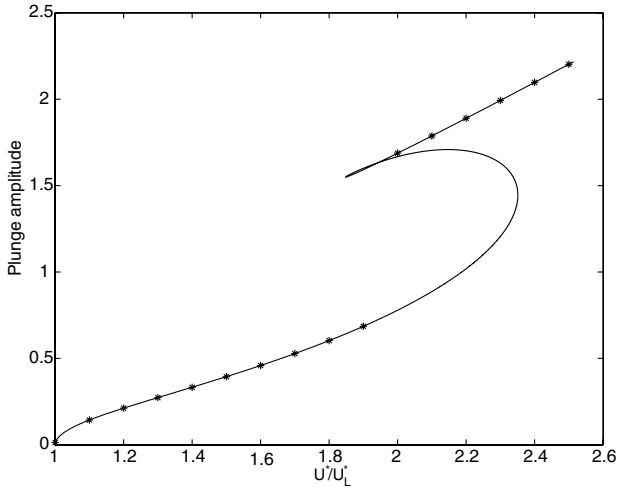

a) Maximum plunge amplitude

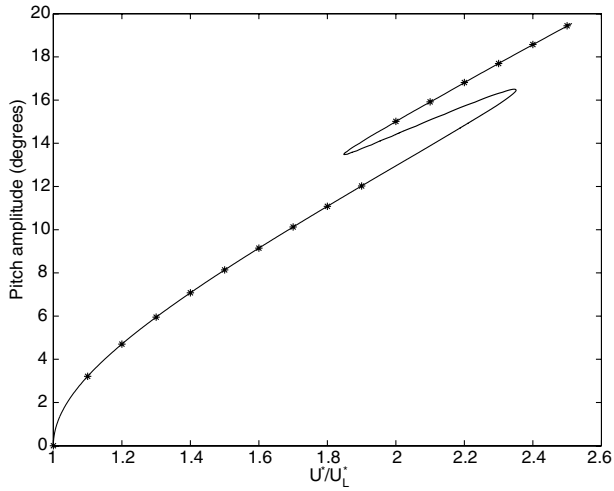

b) Maximum pitch amplitude

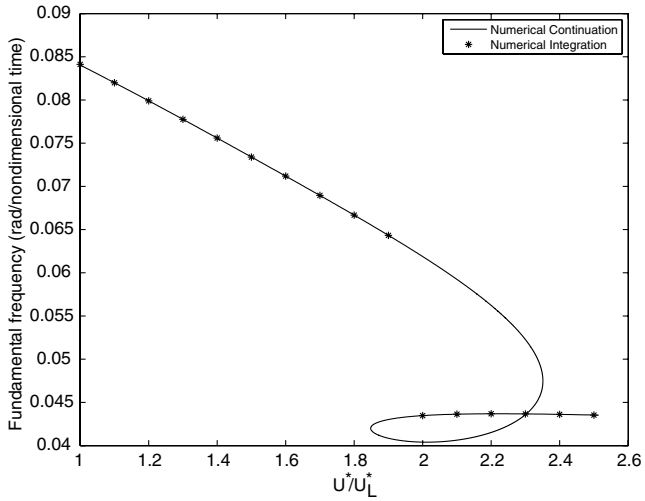

c) LCO frequency

Fig. 2 Numerical continuation results for pitch–plunge airfoil with $\beta = 80$, $\gamma = 0$.

Lee and Liu [27] demonstrated using numerical integration that, when $\gamma = 20$ and all other parameters remain as before, a different jump phenomenon is observed, this time independent of initial conditions. They identified the cause of this jump as a secondary Hopf bifurcation. Numerical continuation can provide evidence that indeed this is the cause of the jump by looking at the eigenvalues of the matrix $(\partial\mathbf{F}/\partial\mathbf{x}(0) \quad \partial\mathbf{F}/\partial T)$ in Eq. (10). When a pair of eigenvalues of this matrix becomes purely imaginary, a secondary Hopf bifurcation occurs. Figure 3 shows the variation of the real part of some of the eigenvalues, obtained when applying the shooting method. It can be seen that one of the real parts becomes zero at $U^*/U_L^* = 1.78$. The LCO amplitude and frequency predictions obtained from numerical continuation are presented in Fig. 4, along with numerical integration results. It can be seen that the jump coincides with the secondary Hopf bifurcation.

VI. Generic Transport Aircraft Model

Although the demonstration of the previous section is interesting, it is important to determine whether continuation approaches can be applied to more realistic and significantly larger models. The model studied in this section is a generic transport aircraft (GTA) as defined in the ZAERO manual [29] and used in several research publications, for example, Karpel et al. [30]. The model was created using MSC-NASTRAN software and includes structural information calculated from a finite element grid and aerodynamic information obtained using the doublet lattice method. The aircraft has a straight rectangular wing and a T tail with a straight rectangular tailplane. Five aerodynamic control surfaces are included, two ailerons, two elevators, and a rudder. No engines are modeled. Figure 5a shows the aerodynamic grid and Fig. 5b the structural grid. The structure is a finite element stick model created using bar elements. The masses are

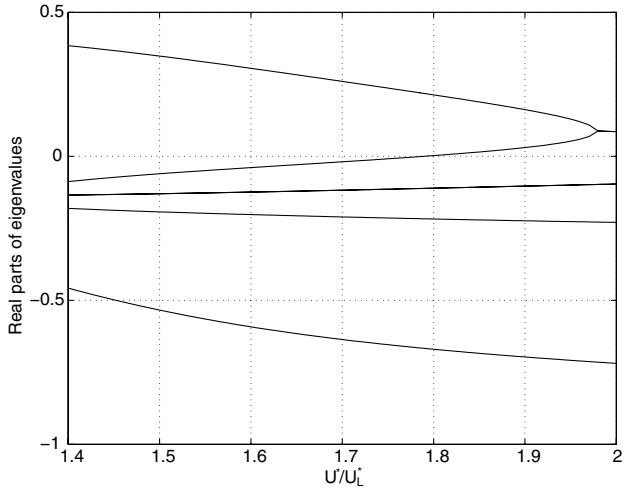

Fig. 3 Evolution of real parts of eigenvalues with airspeed for case $\beta = 80$, $\gamma = 20$.

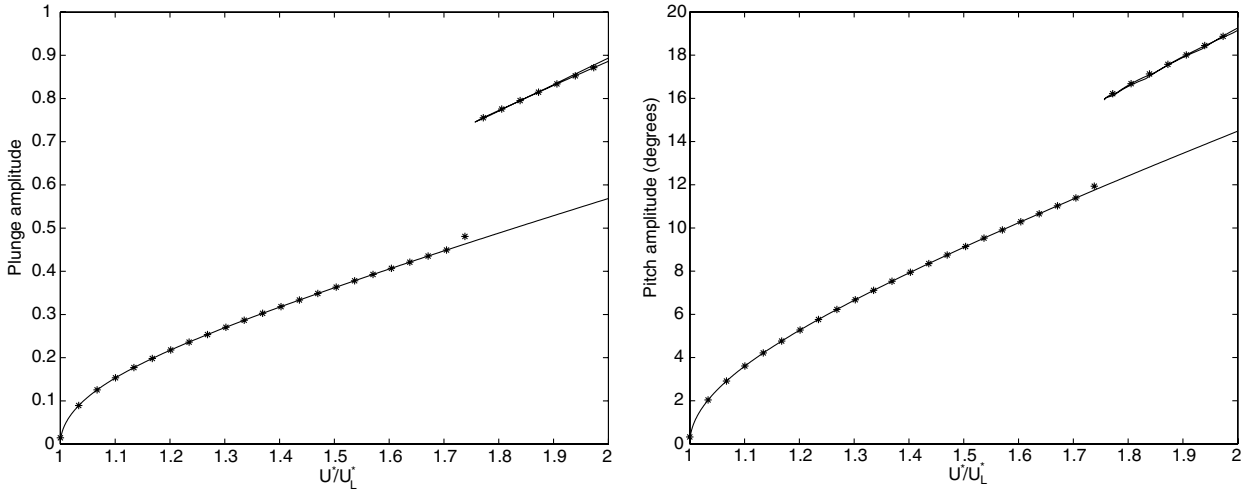

a) Maximum plunge amplitude

b) Maximum pitch amplitude

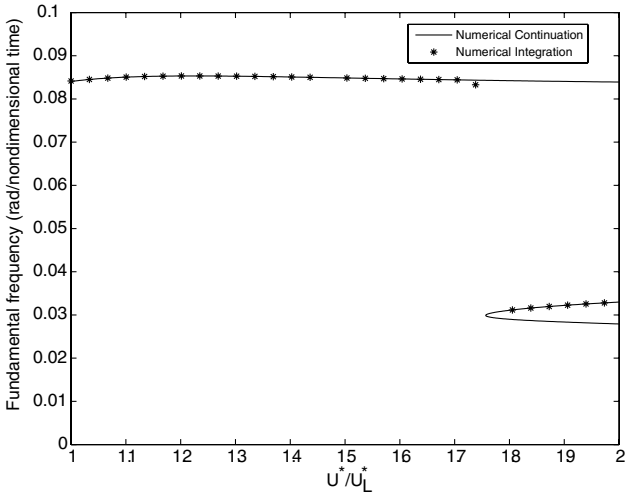

c) LCO frequency

Fig. 4 Numerical continuation results for pitch–plunge airfoil with $\beta = 80$, $\gamma = 20$.

distributed on the nodes to obtain the correct mode shapes and frequencies.

The equations of motion for the GTA are obtained in modal space as

$$\mathbf{M}\,\ddot{\mathbf{q}} + \mathbf{C}\dot{\mathbf{q}} + \mathbf{K}\mathbf{q} = q\mathbf{Q}(\jmath k) \tag{48}$$

where $\mathbf{M}$ is the modal mass matrix, $\mathbf{C}$ is the modal damping matrix, $\mathbf{K}$ is the modal stiffness matrix, $\mathbf{q}$ are modal coordinates, q is the dynamic pressure, and $\mathbf{Q}(\jmath k)$ are the aerodynamic forces, which are functions of the reduced frequency, k. The number of retained modes, n_m, is 7. The equations of motion are transformed to first-order form using Roger's approximation [31]. The aerodynamic forces are written in the form

$$\mathbf{Q}\,(\jmath k) = \mathbf{A}_0 + \mathbf{A}_1 \jmath k + \mathbf{A}_2 (\jmath k)^2 + \sum_{j=1}^{n_l} \mathbf{A}_{2+j} \frac{\jmath k}{\jmath k + \gamma_j} \tag{49}$$

where $\mathbf{A}_j$ are $n_m \times n_m$ real matrices and γ_j are aerodynamic lag coefficients calculated from

$$\gamma_j = -1.7 k_{\max} \frac{j}{(n_l + 1)^2} \tag{50}$$

with $k_{\max}$ being the maximum reduced frequency at which the aerodynamic matrix, $\mathbf{Q}(\jmath k)$, was obtained from NASTRAN and n_l being chosen as equal to 4.

The full first-order equations become

$$\dot{\mathbf{x}} = \begin{pmatrix} -\bar{\mathbf{M}}^{-1}\bar{\mathbf{C}} & -\bar{\mathbf{M}}^{-1}\bar{\mathbf{K}} & \bar{\mathbf{M}}^{-1}\bar{\mathbf{A}}_3 & \bar{\mathbf{M}}^{-1}\bar{\mathbf{A}}_4 & \bar{\mathbf{M}}^{-1}\bar{\mathbf{A}}_5 & \bar{\mathbf{M}}^{-1}\bar{\mathbf{A}}_6 \\ \mathbf{0} & \mathbf{I} & \mathbf{0} & \mathbf{0} & \mathbf{0} & \mathbf{0} \\ \mathbf{0} & \mathbf{I} & -V\gamma_1/b\mathbf{I} & \mathbf{0} & \mathbf{0} & \mathbf{0} \\ \mathbf{0} & \mathbf{I} & \mathbf{0} & -V\gamma_2/b\mathbf{I} & \mathbf{0} & \mathbf{0} \\ \mathbf{0} & \mathbf{I} & \mathbf{0} & \mathbf{0} & -V\gamma_3/b\mathbf{I} & \mathbf{0} \\ \mathbf{0} & \mathbf{I} & \mathbf{0} & \mathbf{0} & \mathbf{0} & -V\gamma_3/b\mathbf{I} \end{pmatrix} \mathbf{x} \tag{51}$$

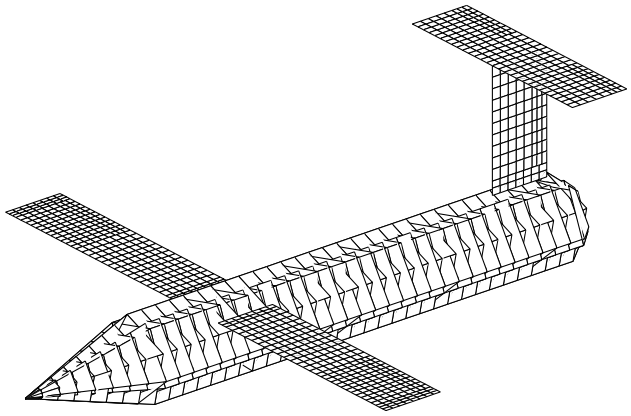

a) Aerodynamic grid

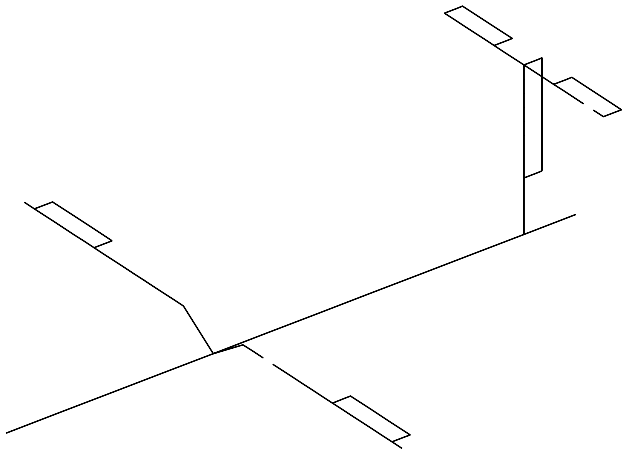

b) Structural grid

Fig. 5 Aerodynamic and structural grids for the GTA model.

where V is the airspeed and

$$\bar{\mathbf{M}} = \mathbf{M} - q\left(\frac{b}{V}\right)^2 \mathbf{A}_2 \qquad \bar{\mathbf{C}} = \mathbf{C} - q\frac{b}{V}\mathbf{A}_1 \qquad \bar{\mathbf{K}} = \mathbf{M} - q\mathbf{A}_0$$

$$\bar{\mathbf{A}}_3 = -q\mathbf{A}_3 \qquad \bar{\mathbf{A}}_4 = -q\mathbf{A}_4 \qquad \bar{\mathbf{A}}_5 = -q\mathbf{A}_5 \qquad \bar{\mathbf{A}}_6 = -q\mathbf{A}_6 \tag{52}$$

The state vector $\mathbf{x}$ is now of the form $\mathbf{x} = [\,\dot{\mathbf{q}}^T \quad \mathbf{q}^T \quad \mathbf{x}_a^T\,]^T$, where $\mathbf{x}_a$ are aerodynamic states. The total number of states in Eqs. (51) is $6n_m = 42$.

Figure 6 shows the resulting modal frequencies and damping ratios obtained from the GTA model for a range of airspeeds at sea level. It can be clearly seen that one of the damping ratios crosses zero at an airspeed of just under 200 m/s, causing flutter.

Structural nonlinearity was included in the GTA model by replacing the springs connecting the aerodynamic control surfaces by nonlinear springs. In this study the case where the right-hand aileron stiffness is nonlinear will be considered. Two nonlinearities are treated, cubic and freeplay. The finite element grid contains $n_g = 678$ nodes. The right-hand aileron angle is given by the difference between the rotations at nodes 563 and 623. To implement nonlinearity in the model the elements of the physical structural stiffness matrix (563,563), (563,623), (623,563), and (623,623) are set to zero and the resulting matrix is transformed to modal coordinates. In the case of cubic stiffness a nonlinear force of the form

$$\mathbf{f}_{\text{nl}} = \mathbf{\Phi}\mathbf{N}K_c\phi^3 \tag{53}$$

is added to the equations of motion, where $\mathbf{\Phi}$ is the $n_m \times n_g$ modal matrix, $\mathbf{N}$ is a $n_g \times 1$ vector whose elements are all zero apart from

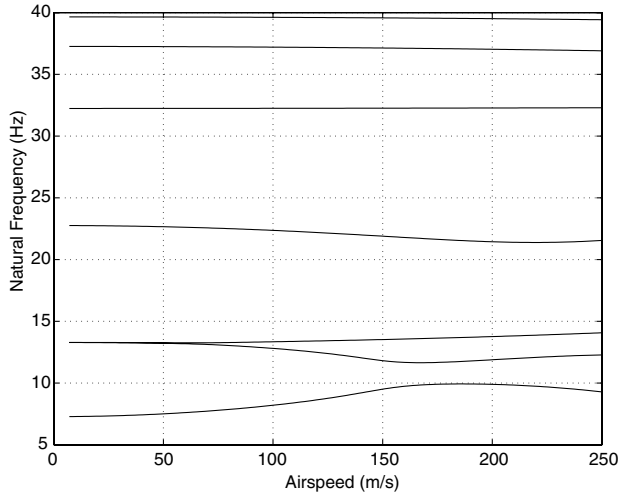

a) Modal frequencies

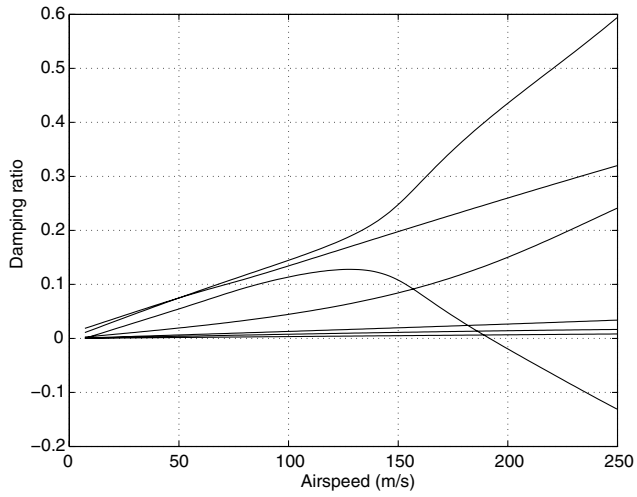

b) Damping ratios

Fig. 6 Modal frequencies and dampings for the GTA model.

elements 563 and 623 which are equal to 1, K_c is a cubic stiffness coefficient, and ϕ is the right-hand aileron angle.

In the case of freeplay stiffness a nonlinear force of the form

$$\mathbf{f}_{\text{nl}} = \mathbf{\Phi}\mathbf{N}\begin{cases} K_f(\phi - \delta) & \text{if } \phi \geq \delta \\ 0 & \text{if } \delta < \phi < \delta \\ K_f(\phi + \delta) & \text{if } \phi \leq \delta \end{cases} \tag{54}$$

is added to the equations of motion where K_f is a stiffness coefficient and δ is equal to half the width of the freeplay region. In the present study the stiffness K_f was chosen equal to that of the linear system whose natural frequencies and damping ratios are plotted in Fig. 6. The freeplay amplitude δ is chosen equal to 0.005 rad, that is, almost 0.3 deg.

Although a single nonlinearity is included in the two models for this demonstration, the number of nonlinearities can be increased for negligible computational cost. For both types of nonlinearity three sets of results are presented, one obtained from the shooting method, one from incremental numerical continuation, and one from simple numerical integration.

A. Shooting Method Results

The shooting method results were obtained using the Runge–Kutta fifth-order scheme mentioned earlier to evaluate Eq. (9) with $m = 251$. Pseudoarclength continuation was chosen and the contraction rate was chosen as $\bar{\kappa} = 0.013$, while the initial arclength increment was set to $\Delta s = 20$. The initial periodic solution was

obtained using Eq. (13). The system Jacobian was updated using Broyden's method.

The bifurcation behavior of the GTA model with cubic stiffness can be observed in Fig. 7. The figure plots the LCO amplitude and period variation with airspeed obtained from the shooting approach (line) and numerical integration (circles). It can be seen that the initial Hopf bifurcation is followed by a slow increase in LCO amplitude and decrease in LCO period. The changes in these two quantities accelerate briefly after 206 m/s until a turning point is reached at 214 m/s. The turning point is a fold, which is easily negotiated by the pseudoarclength technique. The limit cycle becomes unstable and moves toward lower airspeeds until it folds again toward higher airspeeds and becomes stable again. The numerical continuation results were obtained for another three occurrences of this phenomenon and then stopped. Numerical integration results were calculated only for the first two folds.

Figure 7 shows that, although there is only one possible low amplitude limit cycle at airspeeds less than 202 m/s, at higher airspeeds there is a multitude of possible limit cycles with progressively higher amplitudes. This phenomenon can only be fully observed in the numerical continuation results. Numerical integration will only calculate the stable parts of the branch and is much more computationally expensive as integrations must be carried out using a matrix of combinations of initial conditions and airspeeds. The higher number of states makes this an impossible task. In the present study the numerical integration results for the higher amplitude LCOs were obtained using the numerical continuation predictions as initial conditions, only as a check to verify that these are truly attainable LCOs.

The bifurcation behavior of the GTA model with freeplay is dictated by the stability of two underlying linear systems: one with zero stiffness in the right-hand aileron (here called the inner linear system) and one with stiffness K_f (outer linear system). The flutter speed of the inner linear system at sea level is 191.7 m/s. At this airspeed the nonlinear system starts to undergo LCOs with amplitude equal to δ. The outer linear system flutters at 204.1 m/s. At this airspeed the nonlinear system also undergoes divergent oscillations.

Figure 8 plots the LCO amplitude and period against airspeed obtained from the shooting approach (line) together with the numerical integration results (circles). It can be seen that the two sets of results agree quite closely.

The LCO amplitude plot shows that, as expected, LCOs first appear at the flutter speed of the inner linear system and their amplitude is equal to δ. The amplitude then increases with airspeed until it shoots off to infinity at the flutter speed of the outer linear system. The period of the LCOs decreases monotonically with airspeed. It should be noted that the existence of the discontinuity complicates numerical integration in that the time instances at which the nonlinear force switches between one of its three possible values must be calculated to within a suitable tolerance. Various authors have proposed iterative schemes to pinpoint these time instances. As the shooting method also depends on numerical integration, the same considerations should apply. In this author's opinion the exact location of switching time instances is not necessary if the time step is small enough. To test this opinion, the numerical integration results

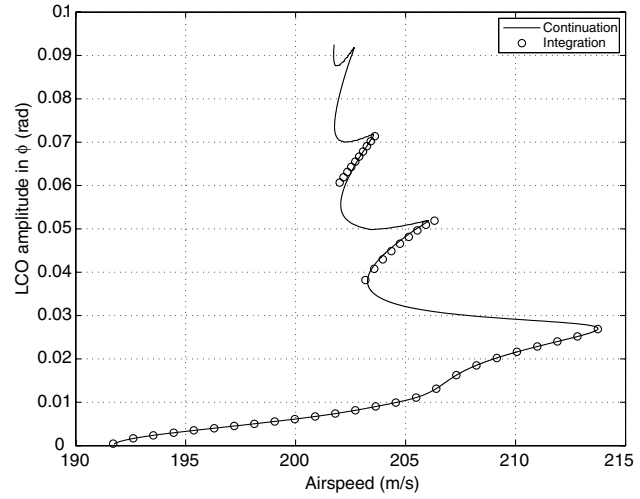

a) LCO amplitude

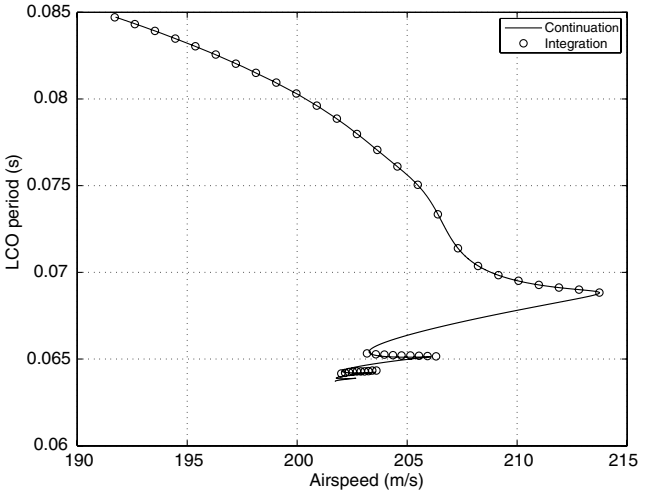

b) LCO period

Fig. 7 LCO amplitude and period for GTA with cubic stiffness (shooting method).

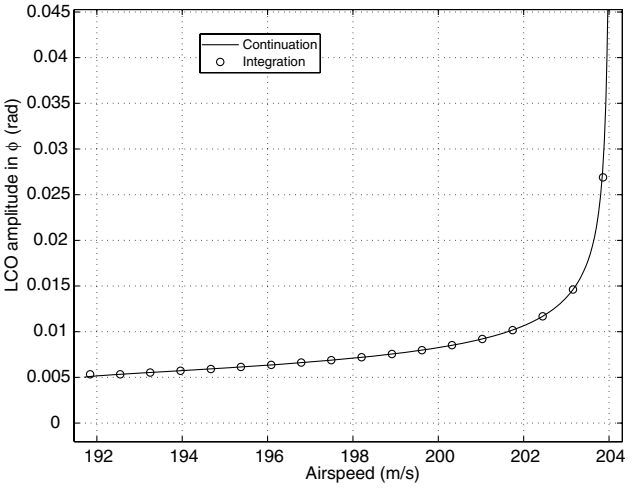

a) LCO amplitude

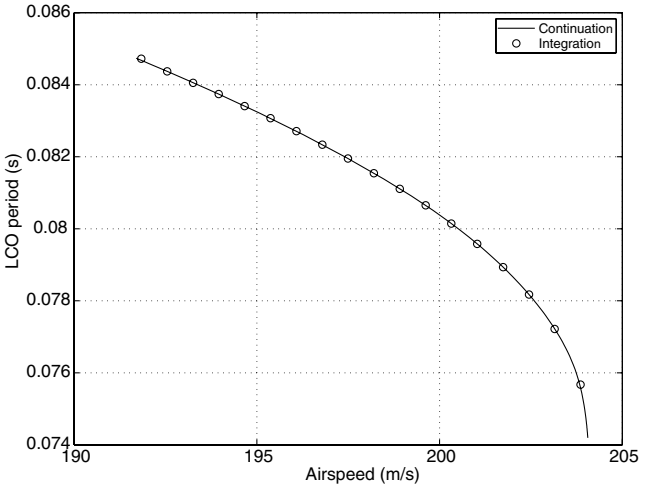

b) LCO period

Fig. 8 LCO amplitude and period for GTA with freeplay stiffness (shooting method).

in Fig. 8 were obtained with switch time location but the numerical continuation results without. The good agreement between the two sets of results seems to support this assertion.

B. Incremental Numerical Continuation Results

Incremental numerical continuation does not solve the full nonlinear equations of motion. It solves Eq. (27), which is a tangential linearization of the nonlinear equations of motion. Equation (27) is only usable when $\Delta\mathbf{x}$, ΔT, and $\Delta\lambda$ are small, for example, $|\Delta\lambda| \ll 1$. For an aeroelastic system, it can be expected that the increments in modal displacements and the period with airspeed are small. However, continuing a solution from, say, 100 to 200 m/s in increments of 0.01 m/s is tremendously wasteful in computational resources. Therefore, λ cannot be chosen to be the airspeed. To speed up the continuation process, λ can be chosen as a scaled airspeed, for example, $\lambda = V/r$, where r is a scale factor. Therefore, $\Delta\lambda = \Delta V/r$ ensures that Eq. (27) is valid while allowing the continuation process to move in reasonably high airspeed increments.

Furthermore, incremental numerical continuation uses forward finite differences to solve for $\Delta\mathbf{x}$, which is a method accurate to $\mathcal{O}(\delta\tau)$. As a consequence, the number of samples in one full period, m, must be sufficiently large to ensure a high level of accuracy.

Incremental numerical continuation was implemented for the GTA using $r = 100$ and various values for m. Pseudoarclength continuation was used with a constant arclength increment set to $\Delta s = 8$. Figure 9 shows the LCO amplitude and period predicted for the GTA with freeplay compared to the numerical integration results. It can be clearly seen that increasing values of m yield significantly improved LCO estimates. The $m = 501$ case fails completely, while the $m = 1001$ case fails to follow the sharp rise in LCO amplitude as the flutter speed of the outer linear system is approached. The $m = 2001$ case is qualitatively correct but inaccurate at higher airspeeds, while the $m = 4001$ case is quite accurate at all airspeeds.

Figure 10 presents the incremental numerical continuation results for LCO amplitude and frequency for the GTA with cubic stiffness. Three sets of results are shown, a continuation result obtained using $m = 4001$, a continuation result calculated from $m = 10,001$, and a numerical integration result. It can be seen that the $m = 4001$ predictions are accurate for the part of the LCO branch before the first fold. After the fold the predictions deteriorate. The $m = 10,001$ curve shows that the section of the branch between the first two folds is predicted quite accurately but the section after the second fold is slightly less accurate. Because of the nature of the incremental continuation method, its accuracy will always drop with increasing arclength s. Having said that, the method offers reasonable accuracy for a comparatively low computational cost.

The significant increase in sampling rate required by the incremental numerical continuation method is not detrimental to the computational efficiency of the method. Even for $m = 10,001$, the approach is significantly faster than the shooting method. The main computational advantage of incremental numerical continuation is, of course, the fact that Newton iterations at every step are not required.

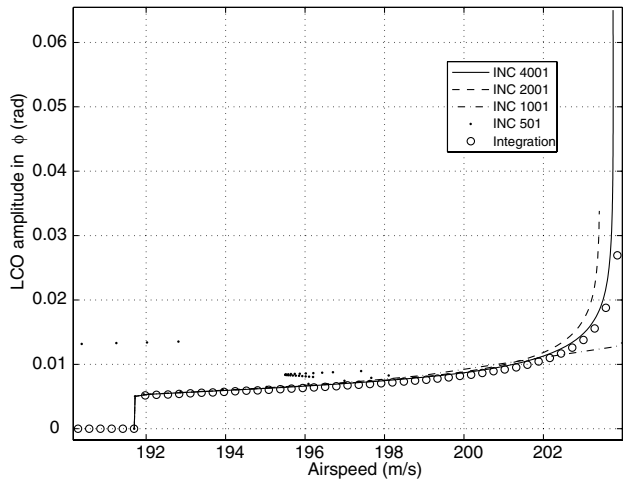

a) LCO amplitude

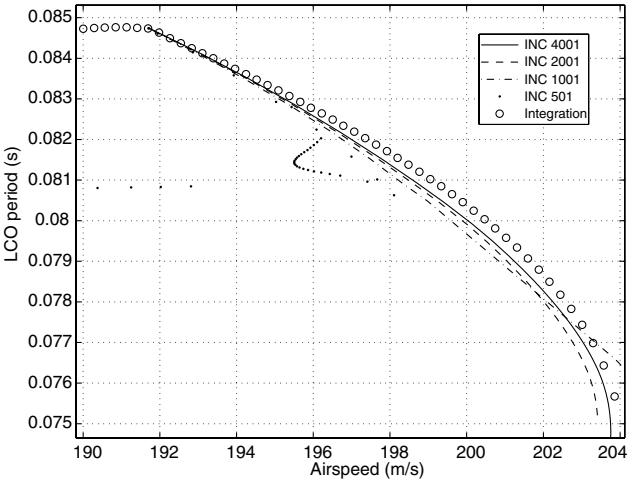

b) LCO period

Fig. 9 LCO amplitude and period for GTA with freeplay stiffness (incremental numerical continuation).

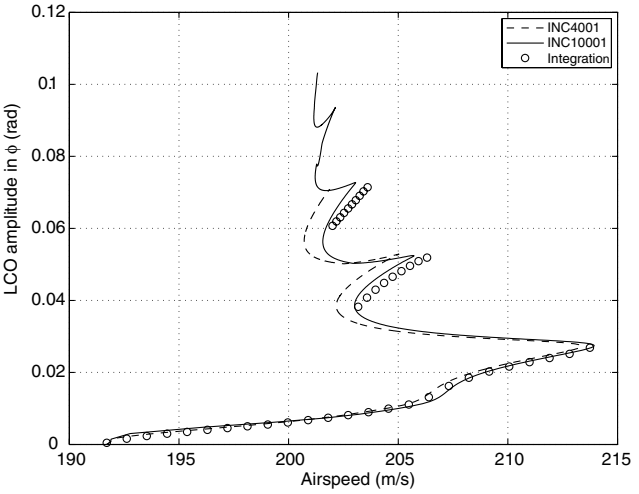

a) LCO amplitude

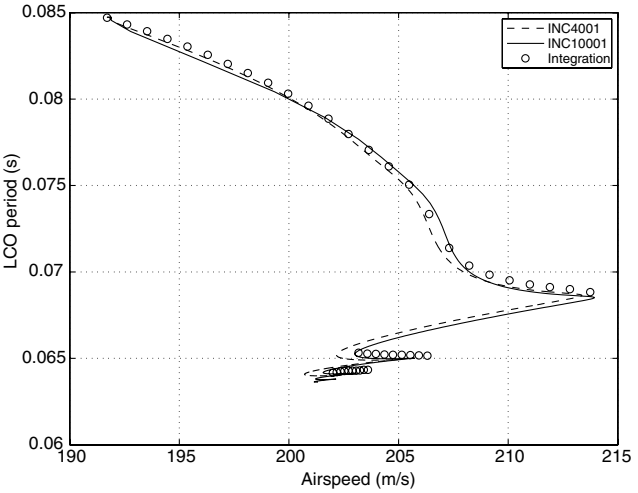

b) LCO period

Fig. 10 LCO amplitude and period for GTA with cubic stiffness (incremental numerical continuation).

VII. Conclusions

A complete methodology has been presented for the prediction of the bifurcation and postbifurcation behavior of nonlinear subsonic aircraft using numerical continuation. Two efficient methods have been described, tailored to the needs of practical aeroelastic systems and coded using simple tools and low computational requirements. The power of numerical continuation was demonstrated on a pitch–plunge airfoil where it was shown that the approach can completely characterize the whole spectrum of system responses, unlike numerical integration. Both continuation methods described in this paper have been demonstrated on a realistic aeroelastic model of a transport aircraft with two types of nonlinearity. The shooting technique is very accurate while the incremental continuation approach offers a reasonable degree of accuracy at lower computational cost.

It should be noted that, as presented here, continuation methods can be applied only to aircraft with linear aerodynamics that can be written in a rational fraction approximation form, because they are only applicable to ordinary differential equations. Nonlinear aerodynamics, such as transonic flow phenomena, can only be adequately modeled by the solution of the Euler or Navier–Stokes equations. Similarly, structural nonlinearities arising from large deformation can only be handled using nonlinear finite element approaches. In such cases numerical continuation must be implemented so that it can solve partial differential equations. This possibility has been discussed [32] but this author has yet to see results from aeroelastic problems. However, considering the huge computational cost of coupled computational fluid dynamics and computational structural dynamics solutions for full aircraft, the application of numerical continuation to such problems may be an important avenue of research.

Appendix: Values of Coefficients in Pitch–Plunge Airfoil Equations of Motion

$$c_0 = 1 + 1/\mu$$

$$c_1 = x_\alpha - a_h/\mu$$

$$c_2 = 2(1 - \psi_1 - \psi_2)/\mu + 2\zeta_\xi \bar{\omega}/U^*$$

$$c_3 = (1 + (1 - 2a_h)(1 - \psi_1 - \psi_2))/\mu$$

$$c_4 = 2(\varepsilon_1\psi_1 + \varepsilon_2\psi_2)/\mu$$

$$c_5 = 2(1 - \psi_1 - \psi_2 + (1/2 - a_h)(\varepsilon_1\psi_1 + \varepsilon_2\psi_2))/\mu$$

$$c_6 = 2\varepsilon_1\psi_1(1 - \varepsilon_1(1/2 - a_h))/\mu$$

$$c_7 = 2\varepsilon_2\psi_2(1 - \varepsilon_2(1/2 - a_h))/\mu$$

$$c_8 = -2\varepsilon_1^2\psi_1/\mu$$

$$c_9 = -2\varepsilon_2^2\psi_2/\mu$$

$$c_{10} = (\bar{\omega}/U^*)^2$$

$$d_0 = x_\alpha/r_\alpha^2 - a_h/\left(\mu r_\alpha^2\right)$$

$$d_1 = 1 + \left(1 + 8a_h^2\right)/\left(8\mu r_\alpha^2\right)$$

$$d_2 = -(1 + 2a_h)(1 - \psi_1 - \psi_2)/\left(\mu r_\alpha^2\right)$$

$$d_3 = (1 - 2a_h)/\left(2\mu r_\alpha^2\right) - (1 + 2a_h)(1 - 2a_h)(1 - \psi_1 - \psi_2)/\left(2\mu r_\alpha^2\right) + 2\zeta_\alpha/U^*$$

$$d_4 = -(1 + 2a_h)(\varepsilon_1\psi_1 + \varepsilon_2\psi_2)/\left(\mu r_\alpha^2\right)$$

$$d_5 = -(1 + 2a_h)(1 - \psi_1 - \psi_2)/\left(\mu r_\alpha^2\right) - (1 + 2a_h)(1 - 2a_h)(\varepsilon_1\psi_1 - \varepsilon_2\psi_2)/\left(2\mu r_\alpha^2\right)$$

$$d_6 = -(1 + 2a_h)\psi_1\varepsilon_1(1 - \varepsilon_1(1/2 - a_h))/\left(\mu r_\alpha^2\right)$$

$$d_7 = -(1 + 2a_h)\psi_2\varepsilon_2(1 - \varepsilon_2(1/2 - a_h))/\left(\mu r_\alpha^2\right)$$

$$d_8 = (1 + 2a_h)\psi_1\varepsilon_1^2/\left(\mu r_\alpha^2\right)$$

$$d_9 = (1 + 2a_h)\psi_2\varepsilon_2^2/\left(\mu r_\alpha^2\right)$$

$$d_{10} = (1/U^*)^2$$

where μ is the airfoil/air mass ratio; x_α is the distance between the elastic axis and the center of mass divided by the half-cord, b; a_h is the distance between the midchord and the elastic axis divided by the half-cord; r_α is a measure of the radius of gyration around the elastic axis; $\psi_1 = 0.165$, $\psi_2 = 0.335$, $\varepsilon_1 = 0.0455$, and $\varepsilon_2 = 0.3$ are constants in Jones's approximation of Wagner's function; ζ_ξ and ζ_α are viscous damping ratios in plunge and pitch, respectively; $\bar{\omega}$ is the ratio of plunge and pitch natural frequencies; and U^* is a nondimensional velocity.

Acknowledgments

The author would like to thank the Engineering and Physical Sciences Research Council of the United Kingdom for its support and G. A. Vio for his help with MSC-NASTRAN modeling.

References

[1] Vio, G. A., and Cooper, J. E., "Limit Cycle Oscillation Prediction for Aeroelastic Systems with Discrete Bilinear Stiffness," *International Journal of Applied Mathematics and Mechanics*, Vol. 1, No. 4, 2005, pp. 100–119.

[2] Liu, L., Wong, Y. S., and Lee, B. H. K., "Application of the Centre Manifold Theory in Non-Linear Aeroelasticity," *Journal of Sound and Vibration*, Vol. 234, No. 4, 2000, pp. 641–659. doi:10.1006/jsvi.1999.2895

[3] Doedel, E. J., Champneys, A. R., Fairgrieve, T. F., Kuznetsov, Y. A., Sandstede, B., and Wang, X. J., "AUTO97-AUTO2000: Continuation and Bifurcation Software for Ordinary Differential Equations (with HomCont): User's Guide," Tech. Rept., Concordia University, Montreal, Canada, 1997–2000.

[4] Govaerts, W., Dhooge, A., and Kuznetsov, Y. A., "MATCONT: A Matlab Package for Numerical Bifurcation of ODEs," *ACM Transactions on Mathematical Software*, Vol. 29, No. 2, 2003, pp. 141–164. doi:10.1145/779359.779362

[5] Roberts, I., Jones, D. P., Lieven, N. A. J., Bernado, M. D., and Champneys, A. R., "Analysis of Piecewise Linear Aeroelastic Systems

Using Numerical Continuation," *Proceedings of the IMechE Part G Journal of Aerospace Engineering*, Vol. 216, No. 1, 2002, pp. 1–11. doi:10.1243/0954410021533382

[6] Beran, P. S., Strganac, T. W., Kim, K., and Nichkawde, C., "Studies of Store-Induced Limit-Cycle Oscillations Using a Model with Full System Nonlinearities," *Nonlinear Dynamics*, Vol. 37, No. 4, 2004, pp. 323–339. doi:10.1023/B:NODY.0000045544.96418.bf

[7] Gee, D. J., "Numerical Continuation Applied to Panel Flutter," *Nonlinear Dynamics*, Vol. 22, No. 3, 2000, pp. 271–280. doi:10.1023/A:1008374401581

[8] Dimitriadis, G., Vio, G., and Cooper, J., "Stability and LCO Amplitude Prediction for Aeroelastic Systems with Structural and Aerodynamic Nonlinearities Using Numerical Continuation," *AVT Symposium on Flow-Induced Unsteady Loads and the Impact on Military Application*, RTO, Budapest, May 2005.

[9] Vio, G. A., Dimitriadis, G., and Cooper, J. E., "Bifurcation Analysis and Limit Cycle Oscillation Amplitude Prediction Methods Applied to the Aeroelastic Galloping Problem," *Journal of Fluids and Structures*, Vol. 23, No. 7, 2007, pp. 983–1011. doi:10.1016/j.jfluidstructs.2007.03.006

[10] Griewank, A., and Reddien, G. W., "Characterization and Computation of Generalized Turning Points," *SIAM Journal on Numerical Analysis*, Vol. 21, No. 1, 1984, pp. 176–185. doi:10.1137/0721012

[11] Doedel, E., Keller, H. B., and Kernevez, J. P., "Numerical Analysis and Control of Bifurcation Problems (1) Bifurcation in Finite Dimensions," *International Journal of Bifurcation and Chaos in Applied Sciences and Engineering*, Vol. 1, No. 3, 1991, pp. 493–520. doi:10.1142/S0218127491000397

[12] Allgower, E. L., and Georg, K., *Numerical Continuation Methods: An Introduction*, Springer–Verlag, New York, 1990.

[13] Broyden, C. G., "A Class of Methods for Solving Nonlinear Simultaneous Equations," *Mathematics of Computation*, Vol. 19, No. 92, 1965, pp. 577–593. doi:10.2307/2003941

[14] Govaerts, W., "Numerical Bifurcation Analysis for ODEs," *Journal of Computational and Applied Mathematics*, Vol. 125, Nos. 1–2, 2000, pp. 57–68. doi:10.1016/S0377-0427(00)00458-1

[15] Rheinboldt, W. C., "Numerical Continuation Methods: A Perspective," *Journal of Computational and Applied Mathematics*, Vol. 124, Nos. 1–2, 2000, pp. 229–244. doi:10.1016/S0377-0427(00)00428-3

[16] Li, M. Y., and Muldowney, J. S., "Phase Asymptotic Semiflows, Poincaŕe's Condition, and the Existence of Stable Limit Cycles," *Journal of Differential Equations*, Vol. 124, No. 2, 1996, pp. 425–448. doi:10.1006/jdeq.1996.0018

[17] Lara, M., and Peĺaez, J., "On the Numerical Continuation of Periodic Orbits," *Astronomy and Astrophysics*, Vol. 389, No. 2, 2002, pp. 692–701. doi:10.1051/0004-6361:20020598

[18] Gerald, C. F., and Wheatley, P. O., *Applied Numerical Analysis*, 5th ed., Addison–Wesley, Reading, MA, 1990.

[19] Lee, B. H. K., Price, S. J., and Wong, Y. S., "Nonlinear Aeroelastic Analysis of Airfoils: Bifurcation and Chaos," *Progress in Aerospace Sciences*, Vol. 35, No. 3, 1999, pp. 205–334. doi:10.1016/S0376-0421(98)00015-3

[20] Lee, B. H. K., Jiang, L. Y., and Wong, Y. S., "Flutter of an Airfoil with a Cubic Restoring Force," *Journal of Fluids and Structures*, Vol. 13, No. 1, 1999, pp. 75–101. doi:10.1006/jfls.1998.0190

[21] Tang, D., Dowell, E. H., and Virgin, L. N., "Limit Cycle Behaviour of an Airfoil with a Control Surface," *Journal of Fluids and Structures*, Vol. 12, No. 7, 1998, pp. 839–858. doi:10.1006/jfls.1998.0174

[22] Liu, L., and Dowell, E., "Harmonic Balance Approach for an Airfoil with a Freeplay Control Surface," *AIAA Journal*, Vol. 43, No. 4, 2005, pp. 802–815.

[23] Millman, D. R., King, P. I., and Beran, P. S., "Airfoil Pitch-and-Plunge Bifurcation Behavior with Fourier Chaos Expansions," *Journal of Aircraft*, Vol. 42, No. 2, 2005, pp. 376–384.

[24] Baldelli, D. H., Lind, R. C., and Brenner, M., "Robust Aeroelastic Match-Point Solutions Using Describing Function Method," *Journal of Aircraft*, Vol. 42, No. 6, 2005, pp. 1597–1605.

[25] Marsden, C. C., and Price, S. J., "Transient and Limit Cycle Simulation of a Nonlinear Aeroelastic System," *Journal of Aircraft*, Vol. 44, No. 1, 2007, pp. 60–70. doi:10.2514/1.21367

[26] Lee, B. H. K., Liu, L., and Chung, K. W., "Airfoil Motion in Subsonic Flow with Strong Cubic Nonlinear Restoring Forces," *Journal of Sound and Vibration*, Vol. 281, Nos. 3–5, 2005, pp. 699–717. doi:10.1016/j.jsv.2004.01.034

[27] Lee, B. H. K., and Liu, L., "Bifurcation Analysis of Airfoil in Subsonic Flow with Coupled Cubic Restoring Forces," *Journal of Aircraft*, Vol. 43, No. 3, 2006, pp. 652–659.

[28] Dimitriadis, G., "Continuation of Higher Order Harmonic Balance Solutions for Nonlinear Aeroelastic Systems," *Journal of Aircraft* (to be published).

[29] "ZAERO Ver. 7.2: Theoretical Manual," ZONA Technology, Scottsdale, AZ, 2004.

[30] Karpel, M., Moulin, B., and Chen, P. C., "Dynamic Response of Aeroservoelastic Systems to Gust Excitation," *Journal of Aircraft*, Vol. 42, No. 5, 2005, pp. 1264–1272.

[31] Roger, K. L., "Airplane Math Modelling Methods for Active Control Design," AGARD, Rept. AGARD-CP-228, 1977.

[32] Davidson, B., "Large Scale Continuation and Numerical Bifurcation for Partial Differential Equations," *SIAM Journal on Numerical Analysis*, Vol. 34, No. 5, 1997, pp. 2008–2027. doi:10.1137/S0036142994273288